nature communications

Article

https://doi.org/10.1038/s41467-025-64551-3

Unconventional bias-dependent tunneling magnetoresistance in van der Waals ferromagnetic/semiconductor heterojunctions

Received: 7 January 2025

Accepted: 19 September 2025

Wenkai Zhu[1,2,8], **Hui Wen**[1,2,8], **Shouguo Zhu**[1,2,8], **Qirui Cui**[3,8], **Shihong Xie**[1,4], **Meng Ye**[1], **Gaojie Zhang**[5,6], **Hao Wu**[5,6], **Xiaomin Zhang**[1,2], **Weihao Li**[1,2], **Yuqing Huang**[1], **Jing Zhang**[1], **Lixia Zhao**[7], **Amalia Patanè**[4], **Haixin Chang**[5,6] ✉, **Lin-Wang Wang**[1] & **Kaiyou Wang**[1,2] ✉

Two-dimensional van der Waals (vdW) ferromagnetic/semiconductor heterojunctions provide an ideal platform for studying and exploiting tunneling magnetoresistance (TMR) effects, due to the versatile band structure of semiconductors and high quality of their interfaces. In all-vdW magnetic tunnel junction (MTJ) devices, both the magnitude and sign of TMR can be tuned by an applied voltage. Typically, as the bias voltage increases, the amplitude of TMR initially decreases, followed by a reversal and/or oscillation in its sign. Herein, we report on an unconventional bias-dependent TMR observed in all-vdW $Fe_3GaTe_2/GaSe/Fe_3GaTe_2$ MTJs, where TMR first increases, then decreases, and ultimately undergoes a sign reversal as the bias voltage increases. By considering the coherent degree of in-plane electron momentum $\mathbf{k}_{\parallel}$ and the decay of the electron wave function through the semiconductor spacer layer, our theoretical prediction successfully explains this unconventional bias-dependent TMR. Consequently, our results offer a deeper understanding of bias-dependent spin-transport in semiconductor-based MTJs and provide new insights into semiconductor spintronics.

Semiconductor spintronics, which primarily focuses on spin injection, manipulation, and detection in semiconducting materials, offers new avenues for designing novel devices such as spin storage, spin logic, spin photodetection and light-emitting devices[1–3]. The discovery of the giant magnetoresistance (GMR) effect in ferromagnet/non-magnet/ferromagnet full-metal heterostructure spin-valve devices, arising from spin-scattering mechanisms, has sparked a surge of interest in spintronic research[4–6]. Subsequently, improved tunneling magnetoresistance (TMR) effect was achieved in magnetic tunneling junction (MTJ) devices based on insulating spacer layers, which mainly rely on spin tunneling mechanisms[7,8]. Numerous studies have demonstrated that the magnitude of TMR is

---

[1]State Key Laboratory of Semiconductor Physics and Chip Technologies, Institute of Semiconductors, Chinese Academy of Sciences, Beijing, China. [2]Center of Materials Science and Optoelectronics Engineering, University of Chinese Academy of Sciences, Beijing, China. [3]Department of Applied Physics, School of Engineering Sciences, KTH Royal Institute of Technology, AlbaNova University Center, Stockholm, Sweden. [4]School of Physics and Astronomy, University of Nottingham, Nottingham, UK. [5]Center for Joining and Electronic Packaging, State Key Laboratory of Material Processing and Die & Mold Technology, School of Materials Science and Engineering, Huazhong University of Science and Technology, Wuhan, China. [6]Wuhan National High Magnetic Field Center, Huazhong University of Science and Technology, Wuhan 430074, China. [7]School of Electrical and Electronic Engineering, Tiangong University, Tianjin, China. [8]These authors contributed equally: Wenkai Zhu, Hui Wen, Shouguo Zhu, Qirui Cui. ✉e-mail: hxchang@hust.edu.cn; kywang@semi.ac.cn

not only related to the spin polarization of the ferromagnetic electrodes, but also closely associated with the band matching between the electrodes and the barrier layer[9,10]. Compared with metallic and insulating barrier layers, semiconducting spacer layers can tune the electron transmission in MTJ devices more efficiently due to their versatile band structures and moderate bandgaps[11,12]. Therefore, the band matching between the semiconductor barrier and the ferromagnetic electrodes can be modulated effectively by bias voltage, thus the TMR effect. However, the efficiency of spin injection in traditional covalently bonded ferromagnetic/semiconductor heterojunction devices is hindered by lattice mismatch and conductivity mismatch between semiconductors and ferromagnetic metals.

Combining novel two-dimensional (2D) van der Waals (vdW) layered ferromagnetic metals with 2D semiconductors via van der Waals forces enables the creation of all-vdW MTJs devoid of lattice mismatch concerns[13–16]. This results in atomically sharp interfaces and minimizes hybridization, thereby enhancing electron tunneling and overcoming the conductivity mismatch. Large TMRs of 300% and 120% have been observed at low temperatures in the all-vdW Fe_3GeTe_2/hBN/Fe_3GeTe_2 and Fe_3GeTe_2/WSe_2/Fe_3GeTe_2 MTJs, respectively[17,18]. Also, a significant room-temperature TMR of 85% has been achieved in the all-vdW Fe_3GaTe_2/WSe_2/Fe_3GaTe_2 MTJs, which surpasses that of traditional covalently bonded ferromagnetic/semiconductor heterojunctions[19,20]. Interestingly, the reported all-vdW semiconductor-based MTJs exhibit a strong bias-dependent TMR effect[12,17–24]: the TMR value tends to decrease with increasing bias, and a sign reversal may occur at large biases. This conventional bias-dependent TMR behavior can be understood by the bias-tuned spin polarization states[17,22,23] and the bias-enhanced spin-dependent scatterings induced by impurities[9].

In this work, we report on a different bias dependence of the TMR in all-vdW MTJs that employ the room temperature perpendicular ferromagnet Fe_3GaTe_2 as the spin injection and detection electrodes, and the semiconductor GaSe as the tunnel barrier. When a bias of 0.5 V is applied between the two electrodes, we observe a maximum TMR of 107% at 10 K and of 25% at room-temperature. In contrast to the previously reported conventional bias-dependent TMR in all-vdW MTJs[17,21,22], an unconventional, M-shaped, bias-dependent TMR behavior is observed. As the bias voltage increases in both positive and negative directions, TMR exhibits symmetrical properties: it first increases, reaches a maximum value, and then rapidly decreases. Subsequently, as the bias voltage continues to increase, its sign reverses. To elucidate the experimental observations, we propose an in-plane momentum ($\mathbf{k}_\parallel$) resolved tunneling model, where both the electron wave function decay and the coherent degree of $\mathbf{k}_\parallel$ through the GaSe spacer layer are taken into consideration. Using this model, we can explain not only the unconventional bias-dependent TMR in Fe_3GaTe_2/GaSe/Fe_3GaTe_2, but also the conventional bias-dependent TMR in Fe_3GeTe_2/GaSe/Fe_3GeTe_2[22]. Our work provides a deep understanding of the bias-dependent TMR in semiconductor-based MTJs, offering a route to the optimization of high-performance all-vdW MTJs.

Results

The all-vdW Fe_3GaTe_2/GaSe/Fe_3GaTe_2 MTJ devices were fabricated using a dry-transfer technique (details are provided in the Experimental Section). The schematic diagram of the device structure and measurement setup is shown in Fig. 1a. The optical image of the device A is shown in Fig. 1b, where the different vdW nanoflakes are outlined with dashed lines of different colors. The atomic force microscope (AFM) measurements indicate that the thickness of the GaSe spacer layer is 10 nm, which corresponds to 11 monolayers[25]. We examined two additional devices with GaSe layer thicknesses of 8 nm (9 monolayers) and 5 nm (6 monolayers), as shown in the Supplementary Information (Figs. S2–4). The bottom and top Fe_3GaTe_2 have different thicknesses (approximately 10 and 20 nm, respectively) to distinguish their coercivities. The nonlinear current-voltage (I-V_b) curves of the device are shown in Fig. 1c at different temperatures in parallel magnetic states. The weak temperature dependence of the current

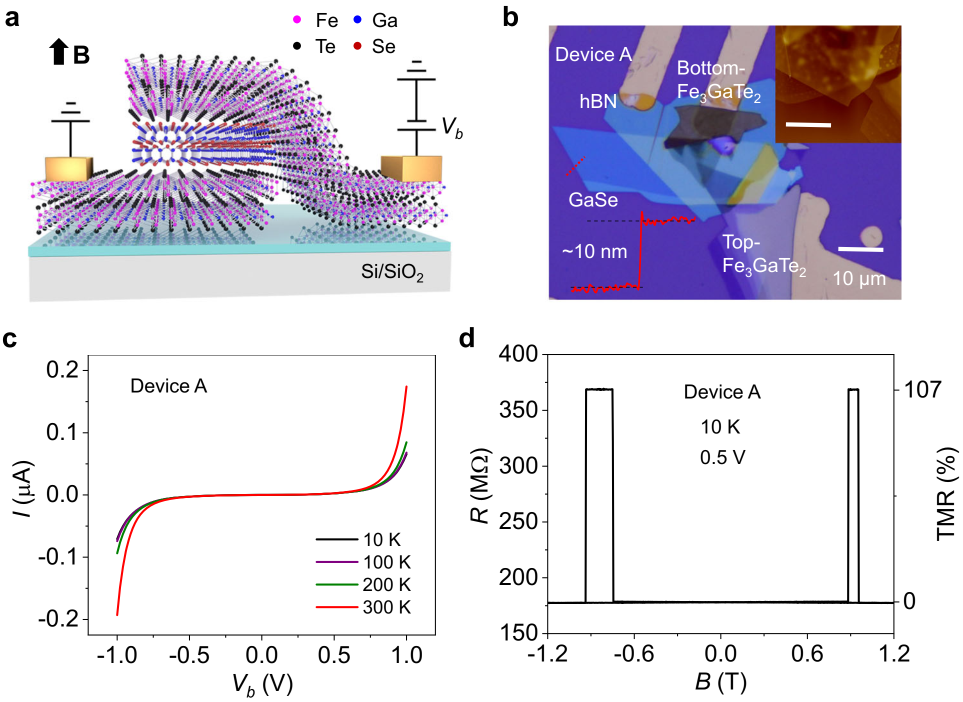

Fig. 1 | Device structure and TMR effect. a Schematic diagram illustrating the Fe_3GaTe_2/GaSe/Fe_3GaTe_2 MTJ device structure and experimental setup. **b** Optical image of device A, where the different vdW nanoflakes are outlined with dashed lines of different colors. AFM measurements indicate that the GaSe layer has a thickness of 10 nm. **c** Temperature-dependent I-V_b curves of device A measured in the parallel state. **d** Resistance hysteresis loop of device A with the bias voltage of 0.5 V at 10 K, indicating a TMR of 107%.

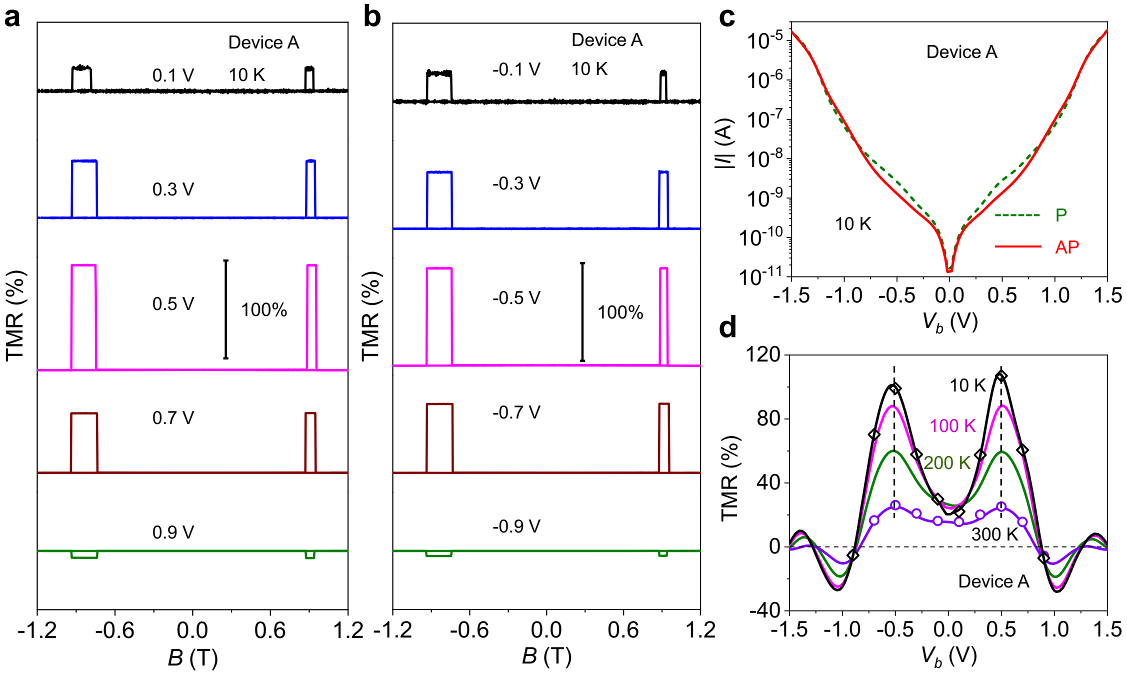

Fig. 2 | Bias-dependent TMR. a TMR curves under positive bias in the range of 0.1 to 0.9 V at 10 K. **b** TMR curves under negative bias in the range of −0.1 to −0.9 V at 10 K. **c** The I-V_b curves of the device in parallel and antiparallel states at 10 K. **d** TMR as a function of the bias voltage at several specific temperatures.

indicates that the transport is dominated by tunneling. By applying a constant bias voltage of 0.5 V on the device at 10 K, as shown in Fig. 1d, we monitored the resistance while scanning the out-of-plane external magnetic field **B**. The resistance of the device in the parallel (P) and antiparallel (AP) magnetic states of the two ferromagnetic layers is 178.1 MΩ and 369.1 MΩ, respectively. This corresponds to a $\mathrm{TMR} = (R_{AP} - R_P)/R_P = I_P/I_{AP} - 1 = 107\%$ at 10 K, where (R_P, I_P) and (R_{AP}, I_{AP}) represent the resistance and measured current values of the device under the P and AP states, respectively. The TMR of the device under the fixed voltage of 0.5 V decreases with increasing temperature, going to zero at 400 K (see Fig. S1), which is due to the decrease in the spin polarization of the ferromagnet. The TMR reaches a value of 25% at room temperature.

We studied the TMR effect of the device under different positive and negative biases, as shown in Fig. 2a, b. The TMR values under different biases are presented in Fig. 2d as open squares. Furthermore, we separately measured the I-V_b curves of the device under P and AP states (Fig. 2c), from which we extracted the TMR as a function of the bias voltage (Fig. 2d), which match well with those obtained from Fig. 2a, b. The TMR of the device first increases and then decreases with the bias voltage, reaching its maximum value at a bias of ±0.5 V. As the bias voltage continues to increase to ±0.9 V, there is a sign reversal in TMR. This M-shaped bias-dependent TMR is different from the conventional TMR behavior mentioned above, which has a maximum value near zero bias, rapidly decreases with increasing bias, and then undergoes a sign reversal. In the two additional devices with different GaSe thicknesses, we also observed a similar M-shaped bias-dependent behavior, verifying the reproducibility of the phenomenon (Figs. S2–4). Both the resistance and TMR of the MTJ devices increase with the increasing GaSe thicknesses from 5 nm to 10 nm. However, in a device with a 12-nm-thick GaSe layer, the TMR signals disappear due to the relatively thick GaSe layer (Fig. S5). Figure 2d shows the bias-dependent TMR curves of the device at several specific temperatures. The M-shape bias-dependent TMR behavior is robust with temperature, with the maximum TMR values around 0.5 V, indicating a stable tunneling mechanism as the origin of the TMR.

Similar unconventional bias-dependent TMR effects have also been observed in MTJs with magnetic barrier layer[26–32] or ferroelectric spacer layer[33], and in resonant tunneling device[34]. These can be attributed to the spin filtering effect of the magnetic tunneling barrier, the ferroelectrically controlled interface spin filtering effect, and the spin-polarized resonant tunneling effect, respectively. Considering the radically different device structures between them and our all-vdW Fe_3GaTe_2/GaSe/Fe_3GaTe_2 MTJ, the theoretical mechanism under our unconventional bias-dependent TMR should be different. There are also some asymmetric bias-dependent TMR behaviors observed in half-metal based MTJs[35,36], which are different from the symmetric bias-dependent TMR behavior in our devices. Thus, a new tunneling model is needed to explain the inner mechanism of the unconventional bias-dependent TMR of the Fe_3GaTe_2/GaSe/Fe_3GaTe_2 MTJ. This model should also be applicable in elucidating the conventional bias-dependent TMR behavior in similar systems, like Fe_3GeTe_2/GaSe/Fe_3GeTe_2[22].

In our previous elastic tunneling models, the band structure of the spacer layer and the scatterings of the in-plane momentum $\mathbf{k}_{\parallel}$ have not been taken into account, which can explain the conventional bias dependent TMR[22,23]. However, these models cannot explain the observed M-shape bias-dependent TMR here. To our knowledge, when an electron tunnels through a thin semiconductor barrier layer, its wave function decay is strongly dependent on $\mathbf{k}_{\parallel}$, which is influenced by the band structure of the barrier layer. Considering the similar crystal structures and relatively small lattice mismatch between Fe_3GaTe_2 and GaSe (details are shown in Fig. S6), we utilize a $\mathbf{k}_{\parallel}$-resolved tunneling model for the TMR calculation within the Fe_3GaTe_2/GaSe/Fe_3GaTe_2 MTJ device. For a very thin spacer layer, the in-plane momentum $\mathbf{k}_{\parallel}$ can be considered as conserved[10]. However, as the spacer layer becomes thicker, the coherent degree of $\mathbf{k}_{\parallel}$ declines with the increasing probability of scatterings. After considering both the band structure of the GaSe spacer layer (related to the electron wave function decay) and the scatterings of $\mathbf{k}_{\parallel}$ (related to the coherent degree of $\mathbf{k}_{\parallel}$), the M-shaped bias-dependent TMR of the Fe_3GaTe_2/GaSe/Fe_3GaTe_2 MTJ device can be well explained. In contrast to the non-equilibrium Green's function method, the $\mathbf{k}_{\parallel}$-resolved tunneling model can offer a more direct and intuitive framework for understanding how the band structure of the barrier layer and the $\mathbf{k}_{\parallel}$ scatterings affect the TMR behavior, which will provide us a deeper insight of the physical mechanisms within the all-vdW tunneling structure. Under an applied voltage, electrons tunnel from the occupied states below the Fermi energy of one electrode to the empty states above the Fermi energy of the other electrode. By taking the up-spin and down-spin as two parallel transmission channels based on the Landauer-Buttiker (LB) formula, the bias-dependent TMR value in this MTJ can be expressed as:

$$\mathrm{TMR}(V_b) = \frac{I_P(V_b) - I_{AP}(V_b)}{I_{AP}(V_b)} * 100\%,$$

$$I_{P/AP}(V_b) \propto \sum_{\delta=\uparrow/\downarrow} \int T^{\delta}_{P/AP} * \left[f(E - eV_b) - f(E)\right] dE, \tag{1}$$

where $\delta = \uparrow/\downarrow$ is the spin coefficient of the tunneling electrons (↑, ↓ represent up-spin and down-spin, respectively), $T^{\delta}_{P/AP}$ represents the spin-dependent transmission function under P/AP states, and $f(E)$ is the Fermi-Dirac distribution at a finite temperature. After considering both the band structure of the GaSe barrier layer and the $\mathbf{k}_{\parallel}$ scatterings, the transmission function of the MTJ device can be written as[37,38]:

$$T^{\delta}_{P/AP} \propto \iint D^{B,\delta}_{P/AP}(\mathbf{k}_{\parallel\mathbf{B}}, E) * D^{T,\delta}_{P/AP}(\mathbf{k}_{\parallel\mathbf{T}}, E) * e^{-2\kappa d} * P(\mathbf{k}_{\parallel\mathbf{B}}, \mathbf{k}_{\parallel\mathbf{T}}) d\mathbf{k}_{\parallel\mathbf{B}} d\mathbf{k}_{\parallel\mathbf{T}},$$

$$P(\mathbf{k}_{\parallel\mathbf{B}}, \mathbf{k}_{\parallel\mathbf{T}}) = \frac{1}{2\pi\sigma^2} e^{-\frac{1}{2\sigma^2}(\mathbf{k}_{\parallel\mathbf{B}} - \mathbf{k}_{\parallel\mathbf{T}})^2}. \tag{2}$$

Here, $\mathbf{k}_{\parallel\mathbf{B}}$ and $\mathbf{k}_{\parallel\mathbf{T}}$ describe the $\mathbf{k}_{\parallel}$ states of the tunneling electrons in the bottom and top electrodes, respectively. $D^{B,\delta}_{P/AP}(\mathbf{k}_{\parallel\mathbf{B}}, E)$ and $D^{T,\delta}_{P/AP}(\mathbf{k}_{\parallel\mathbf{T}}, E)$ are the spin and $\mathbf{k}_{\parallel}$ -resolved density of states under P / AP states of the bottom and top ferromagnetic electrodes[38], which are extracted from the density of states of bulk Fe_3GaTe_2. The decay term $e^{-2\kappa d}$ describes the electron wave function decay during the tunneling process. The attenuation factor $\kappa \sim \sqrt{2m_{\parallel}(U_{\parallel} - E)/\hbar^2}$ is dependent on the band structure of the GaSe barrier layer (for details, see Supplementary Note 1 and Figs. S7–8) and d is the barrier layer thickness. The $\mathbf{k}_{\parallel}$ scattering term $P(\mathbf{k}_{\parallel\mathbf{B}}, \mathbf{k}_{\parallel\mathbf{T}})$ represents the probability of a tunneling electron being scattered from $\mathbf{k}_{\parallel\mathbf{B}}$ state to $\mathbf{k}_{\parallel\mathbf{T}}$ state, which is estimated by two-dimensional Gaussian distribution. The Gaussian distribution factor σ is calculated by a semi classical method with $\sigma = \sigma_0\sqrt{d/\lambda}$. λ is the mean free path of the tunneling electrons in the barrier along the perpendicular direction[39,40], and σ_0 is the Gaussian distribution factor for a single scattering, which can be estimated approximately by the Rutherford scattering model. The schematic diagrams of the $\mathbf{k}_{\parallel}$-resolved tunneling model, both without and with considering the GaSe barrier layer, are shown in Fig. S9.

To provide an intuitive explanation for the M-shaped TMR-V_b behavior, we calculate the $\mathbf{k}_{\parallel}$-resolved conduction channels of the Fe_3GaTe_2/GaSe/Fe_3GaTe_2 MTJ by using the formula $\sum_{\delta=\uparrow/\downarrow} \int D^{B,\delta}_{P/AP}(\mathbf{k}_{\parallel}, E) * D^{T,\delta}_{P/AP}(\mathbf{k}_{\parallel}, E) * \left[f(E - eV_b) - f(E)\right] dE$, which can be derived from Eqs. (1–2) by neglecting both the decay term $e^{-2\kappa d}$ and the $\mathbf{k}_{\parallel}$ scattering term $P(\mathbf{k}_{\parallel\mathbf{B}}, \mathbf{k}_{\parallel\mathbf{T}})$ due to the GaSe barrier layer (Fig. 3a). As the bias voltage increases, the distribution of these conduction channels changes differently for parallel and antiparallel states. Consequently, the TMR values can be affected by the different tunneling probabilities at different $\mathbf{k}_{\parallel}$ points due to the band structure of the barrier layer (the $e^{-2\kappa d}$ term). As illustrated in Fig. 3b, the conduction band of the GaSe barrier layer attains its minimum value at the Γ point, which implies that electrons near the Γ point encounter the lowest barrier height ($U_{\parallel}$, in the attenuation factor). In addition, electrons near the Γ point have the lowest effective mass ($m_{\parallel}$, in the attenuation factor) in GaSe (Fig. S8). These two reasons together lead to the highest tunneling probability (related to the decay term $e^{-2\kappa d}$) near the Γ point. Therefore, the gathering of the conduction channels near the Γ point for the parallel state (Fig. 3a, P state, 0.2 V) will enhance the TMR value. As the bias voltage is further increased, the conduction channels of the antiparallel state also gather towards the Γ point and even become more pronounced (Fig. 3a, AP state, 0.6 & 0.8 V), which results in an M-shaped bias-dependent TMR curve and even negative TMR values within certain bias voltage ranges (for more details, see Supplementary Note 2 and Fig. S10).

After taking the barrier layer GaSe into account, the TMR-V_b relationship of the Fe_3GaTe_2/GaSe/Fe_3GaTe_2 MTJ (mentioned in Fig. 1) is derived from Eqs. (1–2) and presented in Fig. 3c. The unconventional M-shaped TMR-V_b behavior aligns with the experimental results. In contrast, when the GaSe band structure (the $e^{-2\kappa d}$ term) is not considered, a conventional TMR-V_b relationship is observed (Fig. 3d), which verifies the significant $\mathbf{k}_{\parallel}$-dependent spin filtering effect of the GaSe barrier layer. The relatively lower bias voltages of the calculation results than the experiments should be attributed to the voltage-divider effect within the device, where the bias voltage is applied not only on the GaSe barrier layer, but also on the Fe_3GaTe_2 layers and the gaps between the vdW flakes. Furthermore, we calculate the TMR-V_b relationship under different GaSe thickness d and find that the M-shaped bias-dependent TMR behaviors appear only in a particular d range (details see Fig. S11). Therefore, we can conclude that the $\mathbf{k}_{\parallel}$-resolved tunneling process plays a crucial role in the bias-dependent TMR relationship.

In a similar MTJ structure with a GaSe spacer layer of the same thickness (10 nm), we replaced the Fe_3GaTe_2 electrodes with Fe_3GeTe_2 electrodes. The fabricated device exhibited a conventional bias-dependent TMR behavior, consistent with previous observations[22] (details see Fig. S12). To further validate our model, the TMR-V_b relationship of this Fe_3GeTe_2/GaSe/Fe_3GeTe_2 MTJ is also calculated (shown in Fig. S13). Compared with the Fe_3GaTe_2 electrodes, the conduction channel distribution of the Fe_3GeTe_2 electrodes in the P state does not exhibit a more obvious aggregation towards the Γ point than in the AP state as the bias voltage increases. Thus, even when considering both the coherent degree of $\mathbf{k}_{\parallel}$ and the decay of electron wave function in the model, the calculated TMR begins to decrease from zero bias, in contrast to the M-shaped behavior in the Fe_3GaTe_2/GaSe/Fe_3GaTe_2 MTJ. Beyond that, the magnitude of TMR near zero bias and the TMR sign transition point align more closely with experimental observations, and are significantly improved compared to previous theoretical predictions[22].

Discussion

In summary, we observed an unconventional bias-dependent TMR effect in all-vdW Fe_3GaTe_2/GaSe/Fe_3GaTe_2 MTJ devices. As the bias voltage increased in both positive and negative directions, an unconventional M-shaped bias-dependent TMR was observed, with a maximum TMR of 107% at a bias of 0.5 V at 10 K. To uncover the underlying physics of this unconventional bias-dependent TMR, we propose a $\mathbf{k}_{\parallel}$-resolved tunneling model that incorporates both the coherent degree of $\mathbf{k}_{\parallel}$ and the decay of the electron wave function induced by the semiconductor spacer layer. Using this model, not only the unconventional bias-dependent TMR observed in this work, but also the conventional bias-dependent TMR can be elucidated. Our work establishes a solid foundation for understanding the physical origin of the bias-dependent TMR in semiconductor-based all-vdW MTJs. Additionally, the observed M-shaped TMR behavior is not limited to a specific MTJ design. Any MTJ device whose barrier and electrode band structures have similar matching characteristics could exhibit such

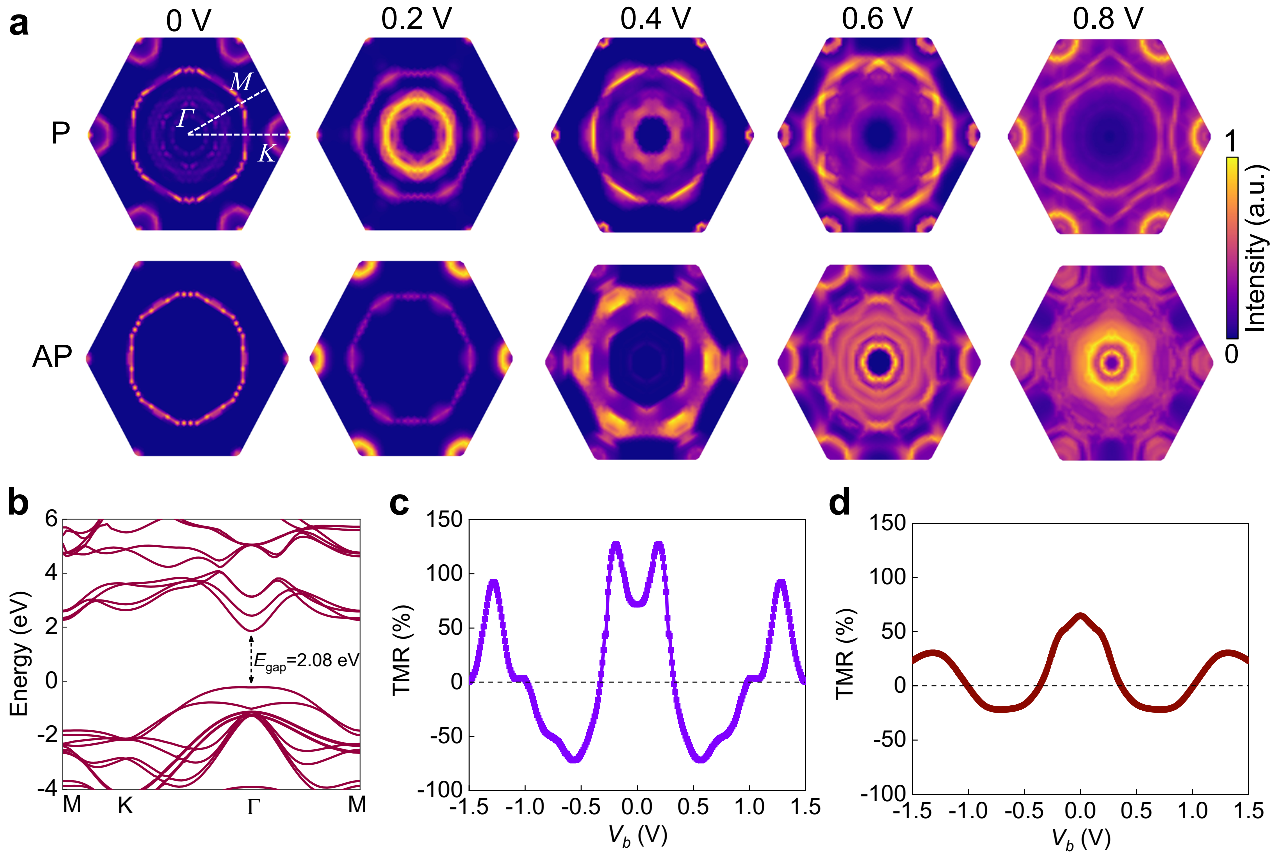

Fig. 3 | Theoretical analysis of bias-dependent TMR. a Schematic diagrams illustrating the **k**-resolved conduction channels of the Fe_3GaTe_2/GaSe/Fe_3GaTe_2 MTJ without considering both the decay term and the **k** scattering term at different bias voltages under P/AP states, respectively. **b** The band structure of bulk GaSe obtained from the first-principles calculations, where both the bottom of the conduction band and the top of the valence band are located at Γ. **c**, **d** The calculated TMR as a function of V_b with (**c**) and without (**d**) considering the band structure of the GaSe barrier layer.

TMR maximum at a specific bias voltage. The universality of this bias-dependent TMR behavior provides more possibilities for the application of all-vdW voltage-controlled MTJ devices.

Methods

MTJ device fabrication

The high-quality vdW single-crystal Fe_3GaTe_2 was grown using the self-flux method. GaSe was purchased from 2D Semiconductors, while WSe_2 and hBN were purchased from HQ Graphene. The metal contact electrodes were pre-patterned by standard photolithography, and Cr (5 nm)/Au (45 nm) layers were deposited onto the Si/300-nm-SiO_2 substrate via an ultrahigh vacuum magnetron sputtering system, followed by a lift-off process. The MTJ devices were fabricated employing a polydimethylsiloxane (PDMS)-assisted 2D dry-transfer method. Initially, the blue tape was used to thin the bulk vdW material. Subsequently, the blue tape was attached to the PDMS/glass sheet to transfer the vdW nanoflakes onto the PDMS. Under an optical microscope, the vdW nanoflakes with appropriate thicknesses were selected based on their optical contrasts (details see the Supplementary Note 3 and Fig. S14). The nanoflakes were then transferred to specific locations on the substrates using a position-controllable dry-transfer method. In the MTJ devices, the bottom layer of Fe_3GaTe_2 had a thickness of approximately 8–12 nm, the top layer of Fe_3GaTe_2 was about 15–20 nm thick, and the semiconductor layer had a thickness ranging from 5 to 10 nm. A protective layer of 30 nm-hBN was applied to the MTJ devices to prevent oxidation. Finally, the MTJ devices were baked at 120° for 10 min after the transfer process to ensure closer contact between the interfaces of the different vdW materials. The entire fabrication process was conducted within a glovebox, which maintained an internal water and oxygen content of less than 0.1 ppm to prevent degradation of the material quality.

Characterization

The AFM (Bruker Multimode 8) was used to characterize the thickness of the vdW nanoflakes.

Magnetoresistance measurements

The electromagnetic transport properties of the device were investigated in a Model CRX-VF Cryogenic Probe Station (Lake Shore Cryotronics, Inc.) with a variable temperature range from 10 K to 500 K and a vertical magnetic field of ±2.5 T. The resistance of the device was monitored by a semiconductor parameter analyzer (Agilent B1500A).

Theoretical calculation

In this study, the first-principles calculations were performed by using the Vienna ab initio simulation package (VASP)[41]. The projector augmented wave (PAW) potentials were applied to the elements[42], and the generalized gradient approximation (GGA) exchange-correlation function was employed[43]. The DFT-D3 correction was used for vdW interaction[44]. The Brillouin zone sampling was performed by using the gamma-centered **k**-meshes (30 × 30 × 6) for the accurate spin-resolved electronic structure calculation.

Data availability

The data that support the findings of this study are available within the article and the Supplementary Information or available from the corresponding author upon reasonable request. All data generated in this study are provided in the Supplementary Information/Source Data file. Source data are provided with this paper.

Code availability

The codes that support the theoretical part of this study are also available from the corresponding author upon reasonable request.

References

1. Julliere, M. Tunneling between ferromagnetic films. *Phys. Lett. A* **54**, 225–226 (1975).
2. Datta, S. & Das, B. Electronic analog of the electro-optic modulator. *Appl. Phys. Lett.* **56**, 665–667 (1990).
3. Dainone, P. A. et al. Controlling the helicity of light by electrical magnetization switching. *Nature* **627**, 783–788 (2024).
4. Baibich, M. N. et al. Giant magnetoresistance of (001)Fe/(001)Cr magnetic superlattices. *Phys. Rev. Lett.* **61**, 2472–2475 (1988).
5. Binasch, G., Grünberg, P., Saurenbach, F. & Zinn, W. Enhanced magnetoresistance in layered magnetic structures with antiferromagnetic interlayer exchange. *Phys. Rev. B* **39**, 4828–4830 (1989).
6. Žutić, I., Fabian, J. & Das Sarma, S. Spintronics: fundamentals and applications. *Rev. Mod. Phys.* **76**, 323–410 (2004).
7. Yuasa, S., Nagahama, T., Fukushima, A., Suzuki, Y. & Ando, K. Giant room-temperature magnetoresistance in single-crystal Fe/MgO/Fe magnetic tunnel junctions. *Nat. Mater.* **3**, 868–871 (2004).
8. Parkin, S. S. P. et al. Giant tunnelling magnetoresistance at room temperature with MgO (100) tunnel barriers. *Nat. Mater.* **3**, 862–867 (2004).
9. Evgeny, Y. T., Oleg, N. M. & Patrick, R. L. Spin-dependent tunnelling in magnetic tunnel junctions. *J. Phys.: Condens. Matter* **15**, R109 (2003).
10. Butler, W. H., Zhang, X. G., Schulthess, T. C. & MacLaren, J. M. Spin-dependent tunneling conductance of Fe|MgO|Fe sandwiches. *Phys. Rev. B* **63**, 054416 (2001).
11. Dolui, K., Narayan, A., Rungger, I. & Sanvito, S. Efficient spin injection and giant magnetoresistance in Fe/MoS_2/Fe junctions. *Phys. Rev. B* **90**, 041401 (2014).
12. Zheng, Y. et al. Spin filtering effect in all-van der Waals heterostructures with WSe_2 barriers. *npj 2D Mater. Appl.* **6**, 62 (2022).
13. Geim, A. K. & Grigorieva, I. V. Van der Waals heterostructures. *Nature* **499**, 419–425 (2013).
14. Gibertini, M., Koperski, M., Morpurgo, A. F. & Novoselov, K. S. Magnetic 2D materials and heterostructures. *Nat. Nanotechnol.* **14**, 408–419 (2019).
15. Zhang, G. et al. Above-room-temperature strong intrinsic ferromagnetism in 2D van der Waals Fe_3GaTe_2 with large perpendicular magnetic anisotropy. *Nat. Commun.* **13**, 5067 (2022).
16. Deng, Y. et al. Gate-tunable room-temperature ferromagnetism in two-dimensional Fe_3GeTe_2. *Nature* **563**, 94–99 (2018).
17. Min, K.-H. et al. Tunable spin injection and detection across a van der Waals interface. *Nat. Mater.* **21**, 1144–1149 (2022).
18. Wang, Z. et al. Tunneling Spin Valves Based on Fe_3GeTe_2/hBN/Fe_3GeTe_2 van der Waals Heterostructures. *Nano Lett.* **18**, 4303–4308 (2018).
19. Zhu, W. et al. Large room-temperature magnetoresistance in van der Waals ferromagnet/semiconductor junctions. *Chin. Phys. Lett.* **39**, 128501 (2022).
20. Pan, H. et al. Room-temperature tunable tunneling magnetoresistance in Fe_3GaTe_2/WSe_2/Fe_3GaTe_2 van der Waals heterostructures. *InfoMat* **6**, e12504 (2024).
21. Wang, Z.-A. et al. Negative-to-positive tunnel magnetoresistance in van der Waals Fe_3GeTe_2/$Cr_2Ge_2Te_6$/Fe_3GeTe_2 junctions. *Chin. Phys. Lett.* **40**, 077201 (2023).
22. Zhu, W. et al. Large and tunable magnetoresistance in van der Waals ferromagnet/semiconductor junctions. *Nat. Commun.* **14**, 5371 (2023).
23. Zhu, S. et al. Voltage tunable sign inversion of magnetoresistance in van der Waals Fe_3GeTe_2/$MoSe_2$/Fe_3GeTe_2 tunnel junctions. *Appl. Phys. Lett.* **124**, 222401 (2024).
24. Jin, W. et al. Room-temperature and tunable tunneling magnetoresistance in Fe_3GaTe_2-based 2D van der Waals heterojunctions. *ACS Appl. Mater. Interfaces* **15**, 36519–36526 (2023).
25. Cao, Y. et al. Strong enhancement of photoresponsivity with shrinking the electrodes spacing in few layer GaSe photodetectors. *Sci. Rep.* **5**, 8130 (2015).
26. Xie, Z.-W. & Li, B.-Z. Bias dependence of the tunneling magnetoresistance in double spin-filter junctions. *J. Appl. Phys.* **93**, 9111–9115 (2003).
27. Yun, L., Bozang, L. & Daosheng, D. Bias Dependence in Spin-Polarized Tunneling of Ferromagnet/Ferromagnetic Insulator (semiconductor)/ferromagnet junctions. *Commun. Theor. Phys.* **31**, 211–214 (1999).
28. Miao, G.-X., Müller, M. & Moodera, J. S. Magnetoresistance in double spin filter tunnel junctions with nonmagnetic electrodes and its unconventional bias dependence. *Phys. Rev. Lett.* **102**, 076601 (2009).
29. Lan, G. et al. Giant tunneling magnetoresistance in spin-filter magnetic tunnel junctions based on van der Waals A-type antiferromagnet CrSBr. *Chin. Phys. Lett.* **40**, 058501 (2023).
30. Song, T. et al. Giant tunneling magnetoresistance in spin-filter van der Waals heterostructures. *Science* **360**, 1214–1218 (2018).
31. Sefrioui, Z. et al. All-manganite tunnel junctions with interface-induced barrier magnetism. *Adv. Mater.* **22**, 5029–5034 (2010).
32. Bruno, F. Y. et al. Insight into spin transport in oxide heterostructures from interface-resolved magnetic mapping. *Nat. Commun.* **6**, 6306 (2015).
33. Tornos, J. et al. Ferroelectric control of interface spin filtering in multiferroic tunnel junctions. *Phys. Rev. Lett.* **122**, 037601 (2019).
34. Zhang, X., Li, B.-Z., Sun, G. & Pu, F.-C. Spin-polarized tunneling and magnetoresistance in ferromagnet/insulator(semiconductor) single and double tunnel junctions subjected to an electric field. *Phys. Rev. B* **56**, 5484–5488 (1997).
35. De Teresa, J. M. et al. Inverse tunnel magnetoresistance in Co/$SrTiO_3$/$La_{0.7}Sr_{0.3}MnO_3$: new ideas on spin-polarized tunneling. *Phys. Rev. Lett.* **82**, 4288–4291 (1999).
36. Marukame, T., Ishikawa, T., Matsuda, K. -i, Uemura, T. & Yamamoto, M. Tunnel magnetoresistance in epitaxial magnetic tunnel junctions using full-Heusler alloy Co_2MnGe thin film and MgO tunnel barrier. *J. Appl. Phys.* **99**, 08A904 (2006).
37. Xiang, X. H., Zhu, T., Du, J., Landry, G. & Xiao, J. Q. Effects of density of states on bias dependence in magnetic tunnel junctions. *Phys. Rev. B* **66**, 174407 (2002).
38. Belashchenko, K. D. et al. Effect of interface bonding on spin-dependent tunneling from the oxidized Co surface. *Phys. Rev. B* **69**, 174408 (2004).
39. Zhang, X. et al. Transient reflectivity measurement of photocarrier dynamics in GaSe thin films. *Appl. Phys. B* **123**, 86 (2017).
40. Abdullaev, G. B., Tagiev, B. G., Mustafaeva, S. N., Gasanov, I. A. & Ibragimova, E. N. Investigation of charge transport processes in amorphous gase films. *Thin Solid Films* **76**, 163–177 (1981).
41. Kresse, G. & Hafner, J. Ab initio molecular-dynamics simulation of the liquid-metal-amorphous-semiconductor transition in germanium. *Phys. Rev. B* **49**, 14251–14269 (1994).
42. Kresse, G. & Joubert, D. From ultrasoft pseudopotentials to the projector augmented-wave method. *Phys. Rev. B* **59**, 1758–1775 (1999).
43. Perdew, J. P., Burke, K. & Ernzerhof, M. Generalized gradient approximation made simple. *Phys. Rev. Lett.* **77**, 3865–3868 (1996).
44. Grimme, S., Antony, J., Ehrlich, S. & Krieg, H. A consistent and accurate ab initio parametrization of density functional dispersion correction (DFT-D) for the 94 elements H-Pu. *J. Chem. Phys.* **132**, 154104 (2010).

Acknowledgements

This work was supported by the National Key Research and Development Program of China (Grant Nos. 2022YFA1405100 and 2022YFE0134600), the Beijing Natural Science Foundation Key Program (Grant No. Z220005), the National Natural Science Foundation of China (Grant Nos. 12241405, 12174384, 52272152, and 12404146). H. W., S. Z., and K. W. thank the very fruitful discussions with Prof. Igor Žutić and Prof. Kirill D. Belashchenko for theoretical model.

Author contributions

K.W. conceived the work. W.Z. fabricated the devices. W.Z., S.Z., S.X., X.Z., and W.L. performed the experiments. W.Z., H.W., S.Z., Q.C., and K.W. analyzed the data. H.W., S.Z., Q.C., M.Y., L.W.W., and K.W. carried out the modeling. H.W., S.Z., and Q.C. performed DFT calculations. G.Z., H.W., and H.C. provided the Fe_3GaTe_2 bulk crystals and conducted the preliminary studies of Fe_3GaTe_2. W.Z., H.W., S.Z., Q.C., Y.H., J.Z., L.Z., A.P., and K.W. wrote the manuscript. All authors discussed the results and commented on the manuscript.

Competing interests

The authors declare no competing interests.

Additional information

Supplementary information The online version contains supplementary material available at https://doi.org/10.1038/s41467-025-64551-3.

Correspondence and requests for materials should be addressed to Haixin Chang or Kaiyou Wang.

Peer review information *Nature Communications* thanks Xiaobin Chen and the other anonymous reviewer(s) for their contribution to the peer review of this work. A peer review file is available.